International Journal of Automotive Technology, Vol. 20, No. 4, pp. 763−777 (2019)
DOI 10.1007/s12239−019−0072−1

pISSN 1229−9138/ eISSN 1976−3832

EFFECTS OF WHEEL CONFIGURATION ON THE FLOW FIELD AND THE DRAG COEFFICIENT OF A PASSENGER VEHICLE

Michael Donald Peter Bolzon[1)*], Simone Sebben[1)] and Alexander Broniewicz[2)]

[1)]Vehicle Engineering and Autonomous Systems, Chalmers University of Technology, Gothenburg 412 58, Sweden
[2)]Environment & Fluid Dynamics Center, Volvo Cars, Volvo Jakobs Väg 418 78, Sweden

(Received 9 August 2018; Revised 4 December 2018; Accepted 10 January 2019)

ABSTRACT−The effects of wheel rotation, rim coverage area, fan spokes, spoke sharpness, and tread pattern on the flow field and drag coefficient of a passenger vehicle were investigated. Force measurements and wake surveys were taken on a 1/ 5th scale passenger vehicle at a Reynolds number of 2.0×10^6. The wake surveys were conducted at three planes. Vorticity, total pressure coefficient, and local drag coefficient plots are presented. Wheel rotation reduced the drag coefficient of all of the wheel configurations tested, which generally agrees with literature. Wheel rotation reduced the front wheel's jetting vortex's drag while increasing the drag from the center of the front wheel to the upper rim track. Reducing the rim coverage area increased the drag coefficient. This increase was attributed to an increased jetting vortex drag and a change in flow separation around the front wheel. The fan spoke rim performed the worst, regardless of rotation. Rounding the spoke edges reduced the drag coefficient of a rotating wheel. The tread pattern slightly reduced the shoulder vortex vorticity and slightly increased the separation around the front wheel.

KEY WORDS : Rotating wheels, Rim aerodynamics, Wake surveying, Jetting vortex

NOMENCLATURE

u	: velocity in x-direction, m/s
v	: velocity in y-direction, m/s
w	: velocity in z-direction, m/s
y	: Y-direction
z	: Z-direction
C_{D_L}	: local drag coefficient
C_{P_t}	: total pressure coefficient
P_S	: static pressure, pa
V	: resultant velocity, m/s
V_∞	: freestream velocity, m/s
ρ	: density, kg/m^3
ω	: vorticity, 1/s

1. INTRODUCTION

Wheels account for approximately 25 % of the total drag coefficient of a passenger vehicle (Schnepf *et al*., 2015). Furthermore, above approximately 70 kph, more than 50 % of the vehicle's power is used in overcoming the vehicle's drag (Hucho, 1998; Barnard, 2001). As such, with regulations becoming increasingly strict (Council of European Union, 2014) and consumer demands rising, reducing the drag of passenger vehicles (and hence increasing its efficiency) is important.

*Corresponding author. e-mail: michael.bolzon@chalmes.se

1.1. Literature Review

A sizable body of literature exists detailing various aerodynamic principles of wheels, both when the wheel is stationary and when it is rotating. One of the most pertinent examples is the effects of wheel rotation; when the flow passes over a stationary wheel, a stagnation point is created on the front of the wheel. It is generally accepted that two relatively large vortices are created at the base of the wheel (termed 'jetting vortices'), and two at the top of the wheel (termed 'top vortices') (Mercker *et al*., 1991; Croner *et al*., 2013; Huminic and Huminic, 2017). Two more vortices are created around the shoulder of the tyre. However, when a wheel rotates, the stagnation point moves upwards, the jetting vortices reduce in size and the top vortices increase in size (Mercker *et al*., 1991; Wäschle *et al*., 2004). Furthermore, wheel rotation also affects the vehicle's general wake (Elofsson and Bannister, 2002). Studies have shown that the effects of front wheel rotation are varied, and the front wheel drag can either decrease or increase, depending on the setup (Wickern and Lindener, 2000; Elofsson and Bannister, 2002; Koitrand and Rehnberg, 2013). In addition, the interaction between local and global effects induced by front wheel rotation is complex; one study surmised, through wind tunnel measurements, that front wheel rotation reduced the drag coefficient by 10 counts, but drag coefficient increases in non-local locations resulted in a minor change to the vehicle's overall drag coefficient (Elofsson and Bannister, 2002). Some limitations to the studies on wheel rotation are that they

typically considered two or three wheel configurations, and that these wheel configurations typically featured conventional rims, such as a 5 spoke rim.

Another pertinent area of wheel aerodynamics is the rim design. The rim coverage area has the greatest effect on the drag coefficient (Landström, 2011; Berg and Brandt, 2018), whereby increasing the rim coverage area decreases the vehicle drag coefficient. Landström (2011) also identified that, the drag coefficient is affected by how the rim is covered; covering the rim from the rim track towards the wheel center is more effective at reducing the drag coefficient than covering the rim from the wheel center towards the rim track, as it reduces the wheel's lower wake size. This investigation was limited in the number of wake planes surveyed, therefore, the evolution of the flow field is unknown. Furthermore, the rims detailed were relatively conventional.

The effect of a fan spoke rim on the drag coefficient is varied with one study reporting little effect (Qiu, 2009) while another study reporting a 9 count increase (D'Hooge *et al*., 2012). The reason for this variability and the general effect of the fan spokes on the flow field are unknown. It should be noted that the fan rims are often designed such that one side of the vehicle features fan rims that draw air out of the wheel house, while the fan rims on the other side of the vehicle draw air into the wheel house. In addition to the fan shaped spokes, the authors were interested in other modifications to the spokes. Namely, the effect of rounding the spoke edges.

The final area of aerodynamic interest that will be detailed is the tyre tread pattern. Numerical results by Hobeika and Sebben (2018a) showed that the edge pattern typically creates small vortices that merge with the jetting vortex and separation zone near the contact patch. These vortices appear to slightly increase the extent of separation. Despite this literature, there is still much uncertainty about how the tread pattern affects the general flow around the wheel and the subsequent drag. Furthermore, experimental results pertaining to the flow field are scarcely available.

1.2. Areas of Investigation

As a result of the above literature review, the following areas of interest were chosen for further investigation: the effects of 1) the wheel rotation, 2) rim coverage area, 3) fan rim, 4) rounding the spoke edges, and 5) tread pattern on the drag coefficient and the flow field.

2. METHODOLOGY

To investigate the above areas of interest, force and flow field measurements were carried out. While the force measurements were relatively simple and easy to perform, the flow field measurements were more difficult and had one overarching constraint; that they had to have a fine spatial resolution. This constraint was chosen as coarse grids make it difficult to compute relevant flow parameters, such as the vorticity. As such, adopting such a coarse grid makes it difficult to ascertain why a given area has such a drag. One of the main goals of this present work is to provide detailed measurements of the flow field. As a result, it was decided to conduct the current campaign in the 1/5th model wind tunnel ("MWT") of the Volvo Cars full scale tunnel. Subsequently, a 1/5th model of a concept vehicle was used; the "Aero 2020". The MWT allowed a 3 mm grid spacing, which corresponded to 15 mm full scale, to be employed. Furthermore, utilising the MWT at the abovementioned grid resolution resulted in sufficient time to investigate nine different wheel geometries.

2.1. 1/5th Model Validity

The most important parameter determining the validity of a scale model experimental setup is the Reynolds number. The experiments were conducted at 30 m/s (the highest velocity possible with this setup), which resulted in a 3.0×10^5 Reynolds number. This fell within the general drag coefficient's Reynolds-number-independent range of a rotating wheel (Hucho, 1998). The Reynolds number based on the vehicle's length was 2.0×10^6.

Another consideration that should be discussed is the wheel rotation method. The MWT did not feature a moving ground, so wheel rotation was done by elevating the Aero 2020 2 mm off of the ground and rotating the wheels through internal motors. The validity of this wheel rotation method was investigated by Arora and Lyu (2016) on this exact model vehicle with the same clearance between the wheels and the ground. They investigated three different wheel configurations on this model Aero 2020 and a full-scale Aero 2020. The full-scale Aero 2020 was installed on a moving ground and the typical Volvo method for rotating the wheels was used (Sternéus *et al*., 2007). The model vehicle's drag coefficient deltas agreed with the full-scale ones. Therefore, it is concluded that the measurements pertaining to the model Aero 2020 with this method of wheel rotation are valid.

The Aero 2020 represents a simplified passenger vehicle; it has a flat underbody, no cooling flow, and no side mirrors. The model wind tunnel had a boundary layer suction zone upstream of the vehicle and a turbulence intensity of 0.5 %.

2.2. Wheel Configurations

Nine different wheel configurations were SLS 3D printed. Eight configurations featured different rims, which are shown in Figure 1; (a) was the same as the 'Covered Treaded' wheel but featured a slick tyre instead of a treaded one. All other configurations featured a treaded tyre. The tread pattern was based on a real production tyre, however, the edge pattern was simplified such that it extended to the shoulder of the tyre instead of wrapping around the shoulder. The rim sizes were 1/5th scaled 21 inch and each wheel featured a brake disc. The rim coverage areas ranged from 33 % to 100 %, as written in parentheses in the Figure

1 caption.

These nine wheel configurations were designed to fulfil the areas of interest for this study listed above. Wheels (b) (Covered Treaded), (c) (5 Spoke Sharp), (f) (5 Spoke Outer Covered), (g) (5 Spoke Inner Covered), and (e) (5 Spoke Closed) were all selected as they exhibited different coverage areas, and they were covered in different fashions. While the Covered Treaded and 5 Spoke Sharp wheels represented opposite ends of the spectrum of coverage area, going from Covered Treaded to 5 Spoke Sharp not only changed the coverage area, but also removed the spokes. Therefore, while this was an expected result, it did not isolate the effects of the coverage area from the spokes. Therefore, in an effort to isolate these effects, the 5 Spoke Closed wheel was developed. This wheel featured a completely covered rim, however, the 5 spoke pattern was still present as the cover was only 1 mm thick, which left 4 mm of the spoke extruding out of the surface. While the synergy between the coverage area and the spokes was ignored with this design, the fundamental effects of the spokes on the flow field were still present. The authors included this design as it is unclear what the primary effects of the spokes on the drag coefficient and flow field are. The 5 Spoke Rounded wheel was exactly the same as the 5 Spoke Sharp wheel, except, while the spokes on the 5 Spoke Sharp wheel were sharp, the spoke edges of the 5 Spoke Rounded Wheel featured a 1 mm radius.

The Covered Slick wheel was designed to investigate the

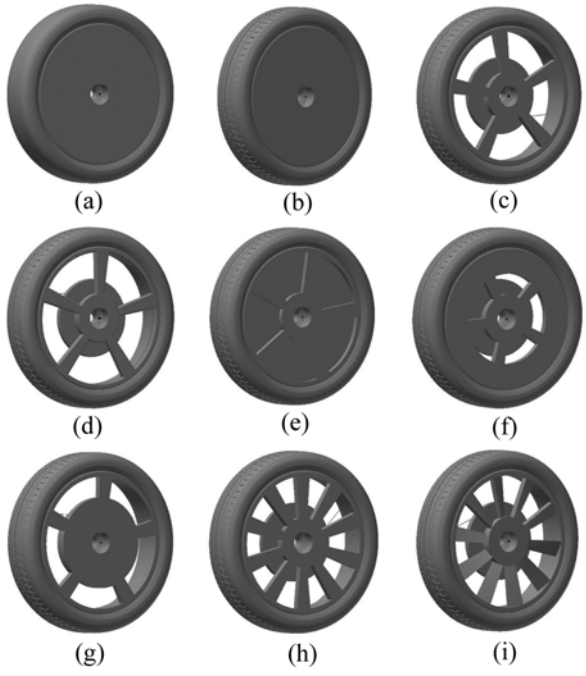

Figure 1. Wheels tested: (a) Covered slick (100 %); (b) Covered treaded (100 %); (c) 5 spoke sharp (33 %); (d) 5 spoke rounded (33 %); (e) 5 spoke closed (100 %); (f) 5 spoke outer covered (76 %); (g) 5 spoke inner covered (62 %); (h) 10 spoke (56 %); (i) 10 spoke fan (56 %).

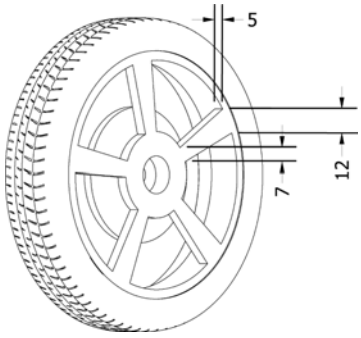

Figure 2. Dimensions of the spoke, mm.

effects of the tread pattern on the aerodynamics of the wheel. The 10 Spoke wheel was the same as the 5 Spoke Sharp wheel except instead of featuring 5 spokes, it featured 10. This wheel was developed for two reasons. The first reason was to determine how increasing the coverage area through more spokes affects the aerodynamics of the wheel. The second reason was to determine the relative effects of the 10 Spoke Fan wheel on the flow field. The fan spokes were right-angled triangles with a flat surface on the inside of the wheel.

The spokes of the 5 Spoke Sharp, 5 Spoke Rounded, and 10 Spoke wheels had thicknesses and widths as shown in Figure 2. The 5 Spoke Closed wheel featured the exact same spokes, except the cover effectively reduced the spoke thickness by 1 mm. The 5 Spoke Outer Covered and 5 Spoke Inner Covered wheels had the same spokes as the 5 Spoke Sharp wheel, except that the area between the spokes were covered to make their respective geometries.

2.3. Force Measurements

The force measurements were taken through a force balance installed underneath the MWT floor. The Aero 2020 was attached to the force balance through four vertical cylinders, which had diameters of 8 mm. Two of the cylinders were located behind the front wheels, and two of them in front of the rear wheels. The forces were taken at a 10 Hz sampling rate for 10 seconds. The drag of all nine wheels were measured, both while the wheels were stationary and rotating.

2.4. Wake Surveys

Wake surveys of all nine wheels were taken with the wheels rotating. Furthermore, wake surveys were also taken of the Covered Slick and 5 Spoke Sharp wheels while stationary. The wake surveys were taken at three streamwise locations; directly upstream of the front right wheel, midway of the front right wheel, and directly behind the front right wheel, as shown in Figure 3. The wake survey planes were 39 mm wide and 180 mm high. Due to practical reasons, the wake surveys started 4 mm away from the rims and 3 mm away from the ground. Measurements were taken for 5 seconds at each point at a

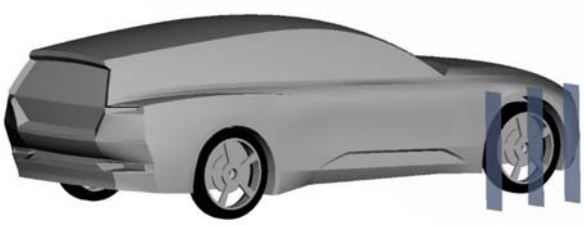

Figure 3. 1/5th scale passenger vehicle used; Aero 2020, and the wake planes surveyed.

sampling frequency of 1000 Hz. The data acquisition unit was a Dewesoft Sirius HD STG-S, which featured a 24-bit resolution. The pressure sensors were SensorTechnics HCLA0025DB. The wind tunnel was held at 21 °C, and all measurements were corrected for any temperature and barometric pressure fluctuations.

The wake surveys were taken with a seven-hole pressure probe, which gave valid measurements within a 70° cone angle (Aeroprobe Corporation, 2015). If 5 % of the measurements at a given grid point were above a 70° cone angle, then the data for the entire grid point were discarded. This cut-off percentage was a conservative choice. These grid points can be seen in the figures below, where the data are missing. Most of the flow angles were within the 70° cone. The seven-hole probe had a tip diameter of 1.6 mm. The total and static pressures, velocity magnitude, and orthogonal velocities were determined through the calibration curve of the particular probe used.

It should be noted that the front plane for the stationary 5 Spoke Sharp wheel and the rotating 5 Spoke Outer Covered wheel were not surveyed due to time restrictions.

2.4.1. Calculated parameters

The streamwise vorticity is defined in Equation (1) and was evaluated using the central difference scheme, as this scheme reduces the error due to noise, compared to a scheme such as the backwards difference scheme, and is less prone to smoothing, compared to a scheme such as the least squares scheme (Hassan *et al*., 2007). As many of the vortices extended beyond the wake survey planes, under the vehicle for example, the vortices' circulations could not be calculated. The vorticity flow fields are presented in the Results section.

$$\omega = \left(\frac{\partial w}{\partial y} - \frac{\partial v}{\partial z}\right) \tag{1}$$

The total pressure coefficient and local drag coefficient were calculated with Equations (2) and (3), respectively. The flow fields detailing these two parameters at each plane surveyed are given in the Results section. While the last two terms (III and IV) of Equation (3) could generally account for the crossflow drag coefficient (thereby resulting in the first two terms, I and II, being assigned to the profile drag coefficient), it would be inaccurate in this situation for two reasons. The first reason is that there is no guarantee that the vortices from the wheel were completely aligned with the freestream direction. The second reason is that the second term (II) in Equation (3) was developed as a correction due to the wind tunnel wall interference on the flow (Maskell, 1973; Wu, 1982). Therefore, it can be concluded that the second term (II) in Equation (3) contains contributions from both the profile and cross flow drag coefficient components. It is possible to implement other equations that would overcome the second reason, such as that presented by Brune (1994), however the first reason would still arise. Furthermore, these alternate equations (Brune, 1994) require that either the entire wake is surveyed, or even worse, that the entire wind tunnel cross-section is surveyed. Neither option was practically feasible in the chosen wake survey plane positions. The last two terms (III and IV) in Equation (3) were calculated for the Covered Tread and 5 Spoke Sharp wheels while rotating and are presented below, however, given the above limitations, these values were only intended as a general indication of the crossflow drag coefficient, and not an accurate decomposition. In addition to the local drag coefficient, the average local drag coefficient of each plane is presented.

$$C_{P_t} = \frac{1/2\rho V^2 + P_S}{1/2\rho V_\infty^2} \tag{2}$$

$$C_{D_L} = \overbrace{(1 - C_{P_t})}^{\text{I}} - \overbrace{\left(1 - \frac{u}{V_\infty}\right)^2}^{\text{II}} + \overbrace{\left(\frac{v}{V_\infty}\right)^2}^{\text{III}} + \overbrace{\left(\frac{w}{V_\infty}\right)^2}^{\text{IV}} \tag{3}$$

3. RESULTS

3.1. Force Measurements

Figure 4 shows the drag coefficients of the stationary

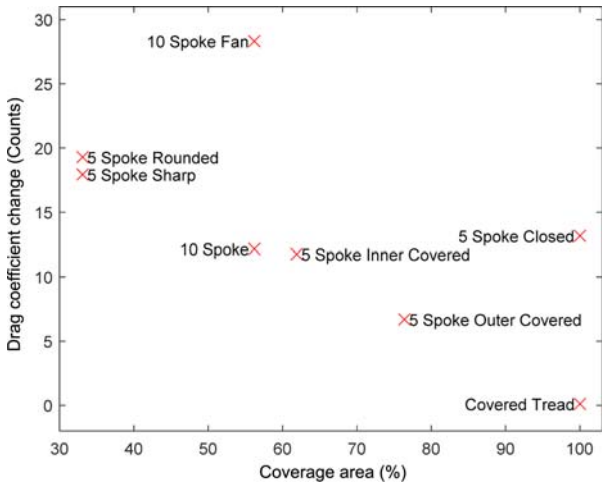

Figure 4. Change in the stationary wheel drag coefficient with respect to the Covered Slick wheel plotted against the coverage area of the rims, counts.

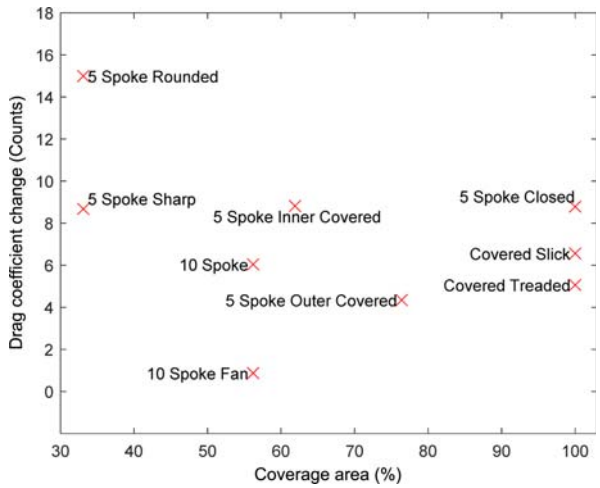

Figure 5. Effect of wheel rotation on the drag coefficient, counts. Plotted against the coverage area of the rims.

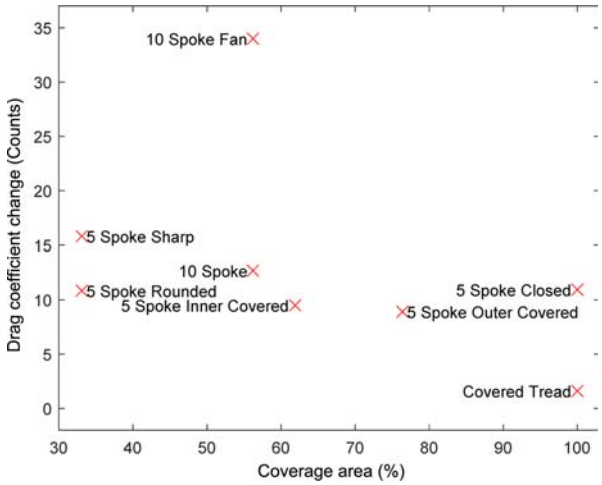

Figure 6. Change in the rotating wheel drag coefficient with respect to the Covered Slick wheel plotted against the coverage area of the rims, counts.

wheels with respect to the Covered Slick wheel, where a positive value indicates that the Covered Slick wheel had a lower drag coefficient. Figure 5 shows the effect of wheel rotation on the drag coefficient of each wheel where a positive value indicates that rotation reduced the drag coefficient. Figure 6 shows the drag coefficients of the rotating wheel configurations with respect to the Covered Slick wheel, where a positive value indicates that the Covered Slick wheel had a lower drag coefficient.

3.1.1. Effect of wheel rotation

Figure 5 shows that wheel rotation reduced all of the wheels' drag coefficients; most of the wheels had between a 4 and 9 count reduction, however, the 10 Spoke Fan wheel had a 1 count reduction, while the 5 Spoke Rounded wheel had a 15 count reduction. These values are within the expected range (Wickern and Lindener, 2000; Elofsson and Bannister, 2002; Koitrand and Rehnberg, 2013). It is interesting to note that the 10 Spoke Fan, Covered Tread and 5 Spoke Outer Covered wheels' drag coefficients were less sensitive to rotation than the Covered Slick wheel's drag coefficient; while the 10 Spoke Fan, 5 Spoke Outer Covered, and Covered Tread wheels could affect the flow through friction *and* the geometric protrusions of the spokes, the Covered Slick wheel could only act on the flow through friction.

Rotation reduced the 5 Spoke Closed and 5 Spoke Sharp wheels' drag coefficient by the same amount. Furthermore, there was no trend between coverage area and the effect of rotation on the drag coefficient.

Generally, wheel rotation resulted in the wheels producing more similar drag coefficients.

3.1.2. Effect of coverage area

A general trend of a decreasing drag coefficient with an increasing coverage area can be seen in Figure 6, which agrees with literature (Landström, 2011). Despite that the 5 Spoke Closed wheel was completely closed, it performed significantly worse than the Covered Tread wheel, with a 9 count greater drag coefficient. This indicates that, while the coverage area impacts the drag coefficient of the wheel, adopting a completely covered rim does not guarantee a low drag configuration; the 5 Spoke Rounded wheel had the same drag coefficient as the 5 Spoke Closed wheel despite a coverage area of only 33 %. This result also shows that the fundamental effect of the spokes significantly affects the drag coefficient. As expected, the 5 Spoke Outer and Inner Covered wheels had relatively low drag coefficients, however, the 5 Spoke Outer Covered wheel had a similar drag coefficient to the 5 Spoke Inner Covered wheel despite having a larger coverage area and being covered from the rim track inwards.

The trend described above also held true for the stationary wheels, as can be seen in Figure 4, however, the 5 Spoke Closed wheel still performed relatively poorly considering that it was completely covered.

3.1.3. Effect of fan rim

The 10 Spoke Fan wheel performed the poorest regardless of whether it was stationary or rotating. The drag coefficient delta between the 10 Spoke Fan and Covered Slick wheels was almost three times as great as the delta between the 10 Spoke and Covered Slick wheels. The 10 Spoke Fan wheel had a 16 and 21 count higher drag coefficient that the 10 Spoke wheel when stationary and rotating, respectively.

3.1.4. Effect of rounding spoke edges

The effect of rounding the spokes' edges was surprising; for a stationary wheel, rounding the spokes' edges had a minor effect and increased the drag coefficient by 1 count.

However, when the wheel was rotating, rounding the spokes' edge reduced the drag coefficient by 5 counts. This indicates that the 5 Spoke Rounded wheel was more sensitive to wheel rotation and hence Reynolds number, which agrees with the literature on square cylinders (Schewe, 2013).

3.1.5. Effect of tread pattern

The tread pattern had no effect on the drag coefficient of a stationary wheel. However, the tread pattern reduced the beneficial effect of wheel rotation on the drag coefficient; the rotating Covered Treaded wheel had a 2 count greater drag coefficient than the rotating Covered Slick wheel. Hobeika *et al*. (2013) found that longitudinal grooves typically reduce the drag coefficient as they equalize the pressure difference between the front and rear of the tyre. However, as these wheels are slightly elevated, this effect is not expected to be present. Therefore, it is likely that this 2 count increase is coming primarily from the lateral grooves, which have displayed similar effects on the drag coefficient as found in this investigation (Hobeika and Sebben, 2018b), or from the effects of the longitudinal grooves directing the flow.

3.2. Wake Surveys

3.2.1. General flow features

The following describes the general flow features found from the wake survey results, and will be referred to throughout the remainder of this study.

Figure 7 shows the streamwise vorticity and the resultant crossflow velocity vectors, the total pressure coefficients, and the local drag coefficients of the Covered Slick and 5 Spoke Sharp wheels while stationary. Figure 8 shows the streamwise vorticity and the resultant crossflow velocity vectors of all rotating wheels at each of the planes surveyed. These plots have been grouped together to facilitate easier comparisons among the different wheel configurations. Figure 9 shows the total pressure coefficient of all rotating wheels at each of the planes surveyed. Similarly, these plots have been grouped together for easier comparisons. Figure 10 shows the local drag coefficient of all rotating wheels at each of the planes surveyed. The colorbars for Figures 8 ~ 10 are the same as the colorbars presented in Figures 7 (b), (d), and (f), respectively. Figure 11 shows the last two terms of Equation (3) (III, IV) for the rotating Covered Treaded and 5 Spoke Sharp wheels. Tables 1 and 2 give the average local drag coefficient of each wheel at each wake survey plane.

3.2.1.1. Front plane

The front plane in all plots of Figure 8 shows a positive vorticity approximately 60 mm from the ground. In addition, the fluid in this region typically moves upwards and away from the vehicle. Thivolle-Cazat and Gilléron (2006) and Hobeika *et al*. (2018b) also found a similar structure. The cause of this vortex is attributed to the tyre shoulder, and therefore is identified as the shoulder vortex. The total pressure coefficient in this region is typically low (high total pressure coefficient deficit), and in some cases the total pressure coefficient becomes negative, which indicates flow separation.

3.2.1.2. Midway plane

Three distinct regions are visible in the midway plane and are labelled on Figure 8 (a). These regions are used when describing Figures 9 and 10 as well. The first region, region 1, is the vorticity in the top portion of the plots in Figure 8, which is likely due to the top vortex. The second region, region 2, is over the middle of the rim; the vorticity found in this region varies among the different wheels. The third region, region 3, is at the bottom of Figures 8 ~ 10, and corresponds to the flow around the base of the wheel. This region is typically associated with the jetting vortex. These three regions have been found in literature (Elofsson and Bannister, 2002; Cogotti, 2008; Söderblom, 2012; Schnepf, 2016). They are also found in the crossflow drag plots in Figure 11; Regions 1 and 3, which correspond to the top and jetting vortices, are of a significantly greater magnitude than region 2.

The vorticity forming in region 1 of the midway plane is almost independent of the wheel configuration; it has a similar magnitude, extent, and movement regardless of the wheel configuration. However, the total pressure and local drag coefficients in this region are significantly different among the nine wheels.

In region 2, the total pressure coefficient is typically below zero for all of the wheels, which indicates flow separation.

3.2.1.3. Back plane

Generally, three lobes form in the back plane total pressure and local drag coefficient plots of all wheels. Lobe 1 is caused by the top vortex and lobe 2 is from the general flow around the wheel. While the jetting vortex is not easily discernible in any of the back plane vorticity plots, lobe 3 is likely caused by it. These lobes have been labelled on Figure 10 (a).

3.2.2. Effects of wheel rotation

Table 1 shows the average local drag coefficient of each plane in Figures 7 (e) and (f).

3.2.2.1. Front plane

Wheel rotation does not significantly affect the average local drag coefficient of the Covered Slick wheel in this plane. However, it does alter the vorticity, total pressure coefficient, and local drag coefficient plot. Furthermore, the effect of rotation on these parameters is the same; it reduces the extent of the given parameter and makes them more rounded.

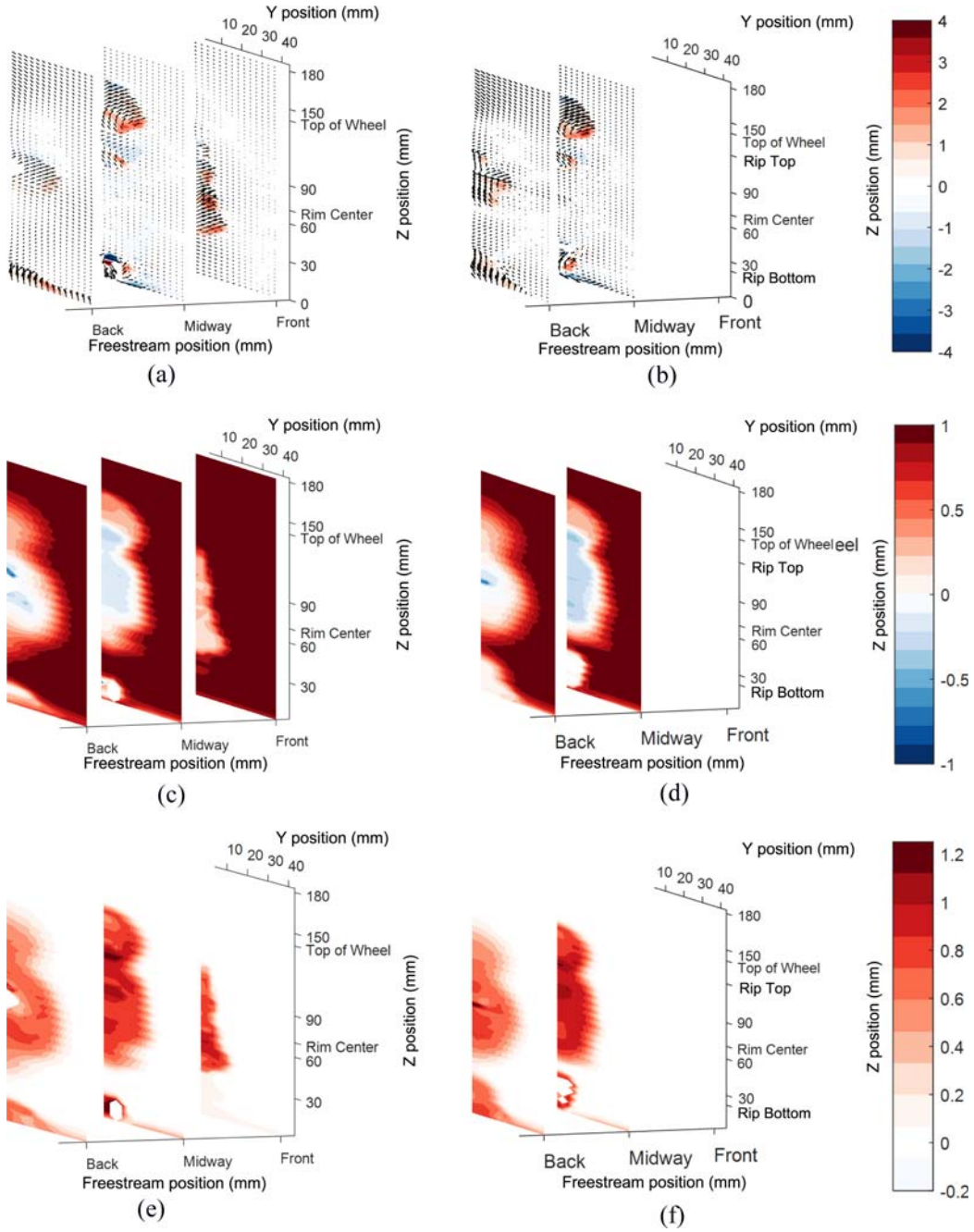

Figure 7. Streamwise vorticity (contours) evolution and flow movement (arrows) (excluding streamwise velocity component): (a) Covered slick stationary; (b) 5 spoke sharp stationary. Total pressure coefficient; (c) Covered slick stationary; (d) 5 spoke sharp stationary. Local drag coefficient; (e) Covered slick stationary; (f) 5 spoke sharp stationary.

3.2.2.2. Midway plane

Wheel rotation has little effect on the vorticity, total pressure coefficient, and local drag coefficient plots of the Covered Slick and 5 Spoke Sharp wheels in region 1.

Rotation has little effect on the Covered Slick wheel's crossflow, total pressure coefficient, and local drag coefficient. However, wheel rotation creates more vorticity and crossflow in the 5 Spoke Sharp wheel's region 2, which results in a greater local drag coefficient.

The jetting vortex of the stationary Covered Slick wheel is of the expected sign, positive, and from the magnitude and the direction of the arrows around the jetting vortex, it appears to be relatively strong. When the wheel is rotating, a dominant negative vortex forms. Rotation also reduces the jetting vortex's local drag coefficient, which, from the vorticity and total pressure coefficient plots, is due to a

Table 1. Average local drag coefficient (dimensionless) of the stationary Covered Slick and 5 Spoke Sharp wheels' planes.

Wheel configuration	Front plane local drag coefficient average	Midway plane local drag coefficient average	Back plane local drag coefficinet average
Covered slick	0.092	0.273	0.236
5 spoke sharp	N/A	0.281	0.260

reduction in both the profile and crossflow drag components. For the stationary 5 Spoke Sharp wheel's region 3, much of the flow has a flow angle greater than 70°, therefore, a comparison between the stationary region 3 and the rotating region 3 is difficult.

Rotating the Covered Slick wheel results in a 13 % reduction in the average local drag coefficient. Rotating the 5 Spoke Sharp wheel results in a 30 % increase in the average local drag coefficient, however, this number is artificially high due to the lack of contribution from the jetting vortex of the stationary wheel.

3.2.2.3. Back plane

Rotation increases the average local drag coefficient of each wheel by approximately 13 %. However, these increases occur for different reasons. Rotation increases the vorticity of the Covered Slick wheel, whereas it reduces the vorticity of the 5 Spoke Sharp wheel. Furthermore, while for the Covered Slick wheel rotation preserves the shape of the three lobes found in the stationary local drag coefficient, these lobes become less defined for the 5 Spoke Sharp wheel.

3.2.3. Effects of rim opening

3.2.3.1. Front plane

The front plane total pressure coefficient plots in Figure 9 show that typically the covered rim wheels have more elongated total pressure coefficient deficits, which extend up the front plane more than the open rims. This elongation is also evident in the local drag coefficient plots in Figure 10, and appears to be developed by covering more of the outer region of the rim, as this elongation is also visible for the 10 Spoke wheel but not for the 5 Spoke Inner Covered wheel.

3.2.3.2. Midway plane

When the rim is open (except for the 5 Spoke Outer Covered rim), a large region of positive vorticity forms in region 2, whereas when the rim is covered, significant amounts of positive and negative vorticity form. The positive vorticity typically coincides with the fluid moving towards the wheel, while no general flow direction is associated with the negative vorticity regions, as indicated by the arrows in Figure 8. Additionally, the area where the total pressure coefficient is below zero is typically greater for the open rims than the covered rims, as shown in Figure 9. Therefore, more flow separation occurs over the open rims than the covered rims. As a result of the greater flow separation, the local drag coefficient in region 2 is typically higher for the open rims than the covered rims, as seen in Figure 10. Expectedly, the open rim in Figure 11 has a greater crossflow drag than the covered rim.

The rim configurations with openings near the rim track have only positively signed vorticity in region 3 (except the 5 Spoke Rounded wheel). However, when the rims are covered near the rim track, for example the 5 Spoke Outer Covered wheel, a region of negative vorticity adjacent to the positive vorticity occurs. It is unclear why this negative vorticity occurs, as the arrows do not show any general patterns among the rims that display this negative vorticity. Furthermore, the wheels with openings near the rim track all exhibit jetting vortices of higher vorticity than the wheels without these openings. The total pressure coefficient deficit is also slightly higher and encompasses a larger area when only positive vorticity is present, which agrees with the data presented in Schnepf (2016). The negative vorticity reduces the local drag coefficient in region 3, which is likely due to both a reduction in the profile and crossflow drag components.

The 5 Spoke Closed wheel had a similar total pressure coefficient plot to the Covered Treaded wheel, indicating a similar flow separation pattern. The crossflow of the 5 Spoke Closed wheel is more than the Covered Treaded wheel, but less than the 5 Spoke Sharp wheel.

The covered rims reduce the average local drag coefficient in this plane by up to 35 %. Therefore, it is concluded that this plane generates much of the difference in the drag coefficient between the covered and open wheels presented above.

3.2.3.3. Back plane

The open rims typically exhibit almost no noteworthy regions of vorticity in the back plane, whereas the covered rims do. In addition, the covered rims usually experience more flow moving away from the vehicle than the open rims. Furthermore, the covered rims typically exhibiting greater total pressure coefficient deficits than the open rims.

Additionally, the general shape of the local drag coefficient plots in Figure 10 are largely determined by whether the wheels feature covered rims or not; the wheels with covered rims typically have more distinct features with three lobes forming. On the other hand, the wheel configurations with open rims typically feature less defined features, which agrees with Schnepf (2016).

The accentuated local drag coefficient near the ground of the 5 Spoke Closed wheel increases the average local drag coefficient of this wheel, such that it is almost the same as the 5 Spoke Sharp wheel. This drag is attributed to the

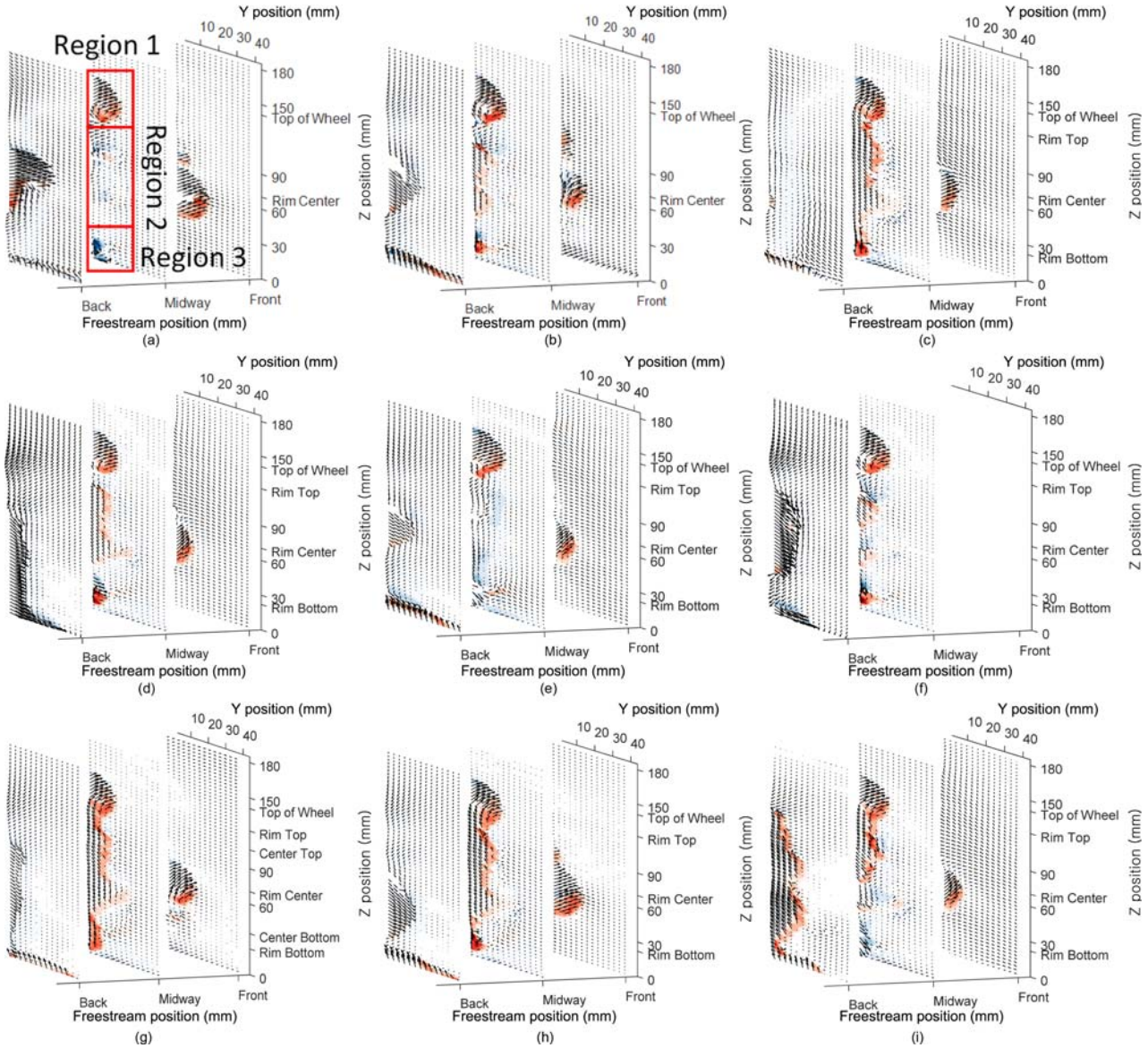

Figure 8. Streamwise vorticity (contours) evolution and flow movement (arrows) (excluding streamwise velocity component): (a) Covered slick; (b) Covered treaded; (c) 5 spoke sharp; (d) 5 spoke rounded; (e) 5 spoke closed; (f) 5 spoke outer covered; (g) 5 spoke inner covered; (h) 10 spoke; (i) 10 spoke fan.

jetting vortex, despite not being discernible in the upstream planes.

Similar to the midway plane (3.2.3.2.), covering a rim typically reduces the average local drag coefficient, with reductions up to 26 % seen.

3.2.4. Effects of 10 spoke fan configuration

The wake surveys were taken on the side of the vehicle that corresponded to the fan rim drawing air out of the wheel house.

3.2.4.1. Front plane

The 10 Spoke Fan wheel produces a similar average local drag coefficient to the 10 Spoke wheel. Minor changes in the vorticity, total pressure coefficient, and local drag coefficient plots exist.

3.2.4.2. Midway plane

In the midway plane, the 10 Spoke Fan wheel does not exhibit a typical jetting vortex. Despite this, the total pressure coefficient and local drag coefficient of the 10 Spoke Fan wheel in region 3 are very similar to the 10 Spoke wheel.

The 10 Spoke Fan wheel has a slightly lower total pressure coefficient in region 2. Furthermore, the vorticity field of the 10 Spoke Fan wheel is very interesting as the

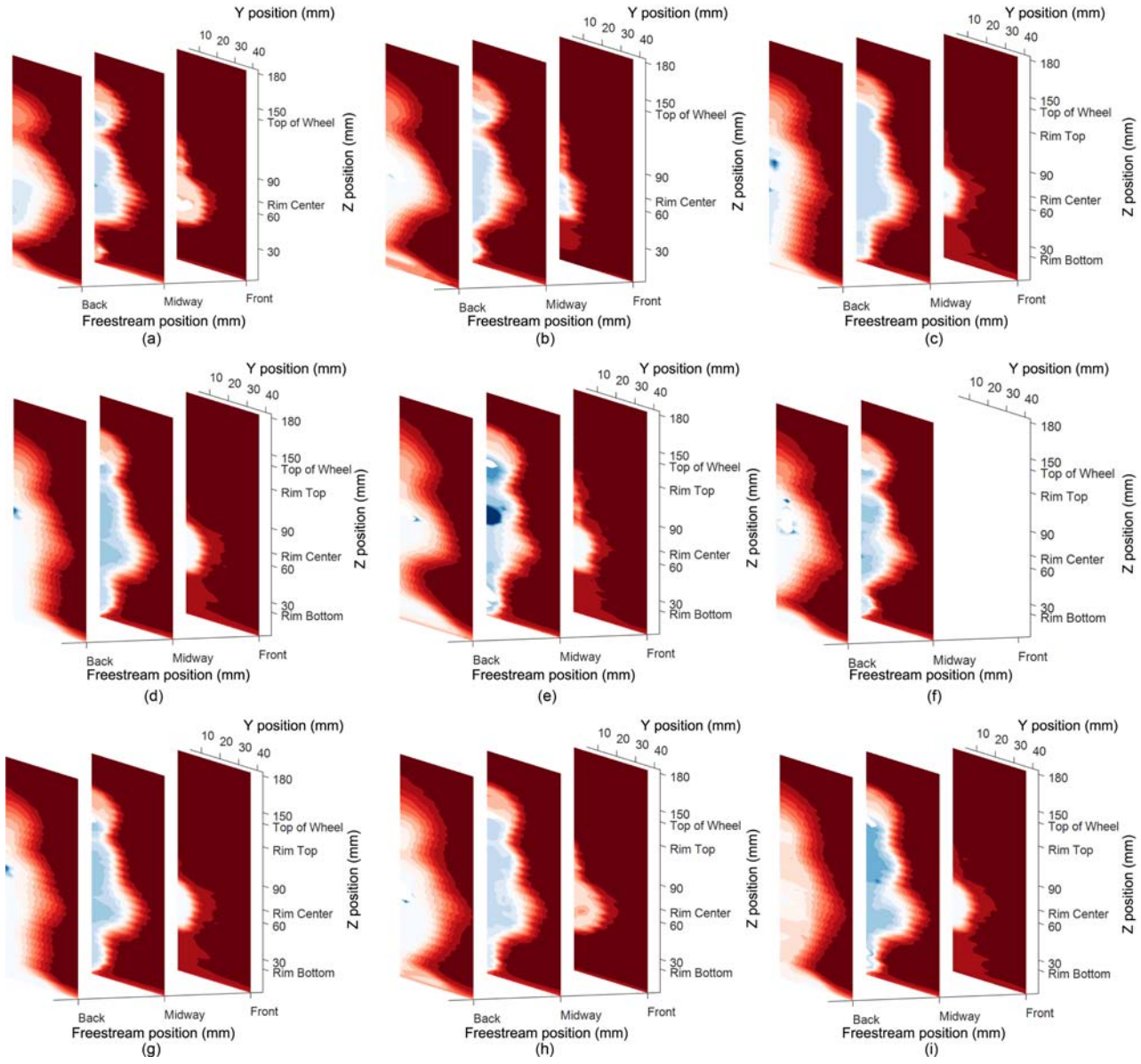

Figure 9. Total pressure coefficient: (a) Covered slick; (b) Covered treaded; (c) 5 spoke sharp; (d) 5 spoke rounded; (e) 5 spoke closed; (f) 5 spoke outer covered; (g) 5 spoke inner covered; (h) 10 spoke; (i) 10 spoke fan.

lower half approximates the fields of the covered rims, while the top half approximates the fields of the open rims. Despite these differences, no appreciable changes in the local drag coefficient plot exists.

The average local drag coefficient of the 10 Spoke Fan wheel is very similar to the 10 Spoke wheel in this plane.

3.2.4.3. Back plane

The 10 Spoke Fan wheel's vorticity in the back plane is markedly different to the 10 Spoke wheel, and every other wheel as well. While the 10 Spoke wheel has little vorticity, the 10 Spoke Fan wheel displays positive vorticity spanning the entire wheel. This vorticity also segregates the flow that is moving towards the vehicle from the flow that is not. Furthermore, the flow moving towards the vehicle has a crossflow velocity of up to 13.2 m/s. These differences are reflected in the total pressure coefficient plot in Figure 9; while the general shape is similar to the 10 Spoke wheel plot, the magnitude is slightly higher, which indicates flow reattachment. The local drag coefficient is typically higher than any of the other configurations, which also agrees with the values in Table 2. As the crossflow velocities are higher for the 10 Spoke Fan wheel than the 10 Spoke wheel, it is reasonable to conclude that the increased local drag coefficient is due to a greater crossflow drag.

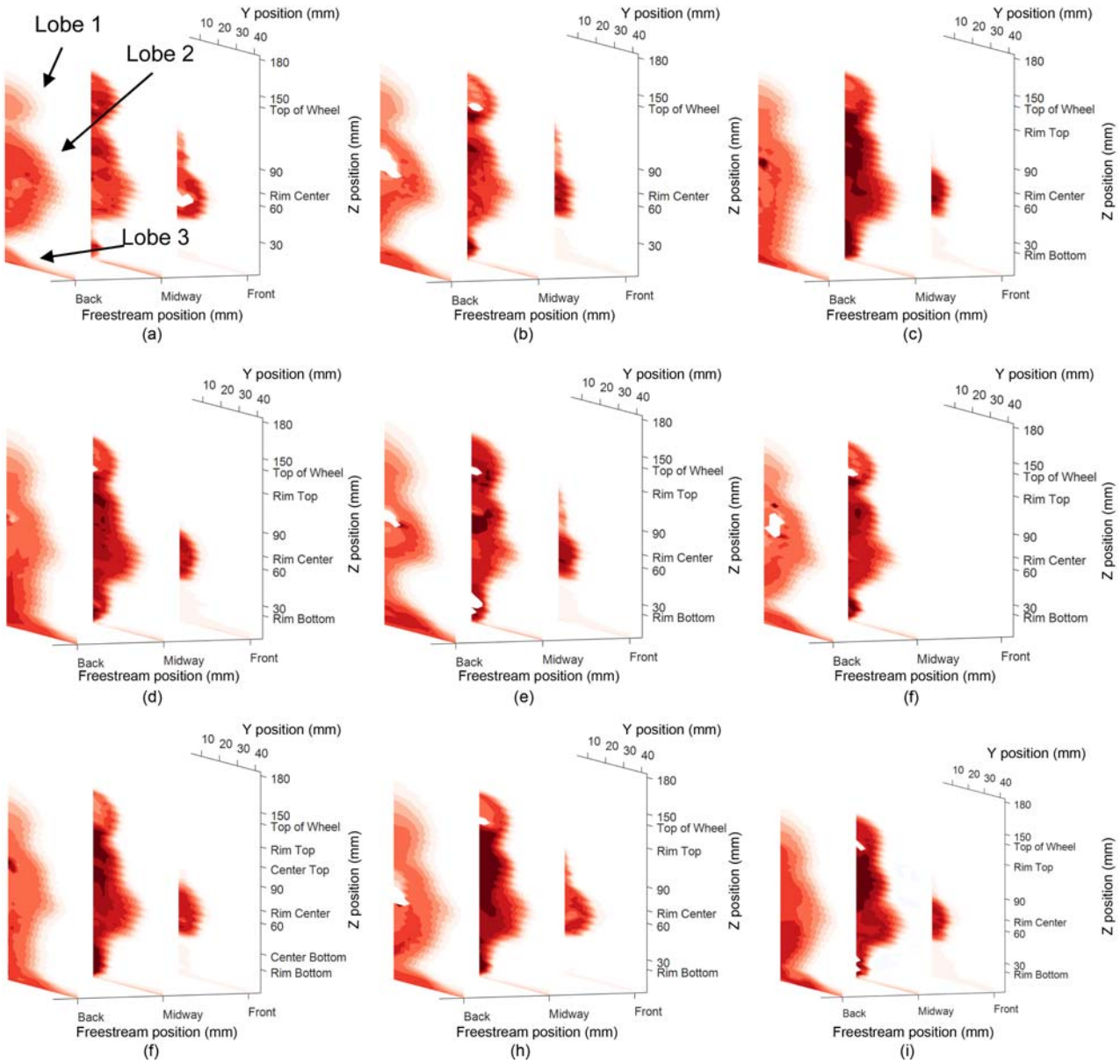

Figure 10. Local drag coefficient: (a) Covered slick; (b) Covered treaded; (c) 5 spoke sharp; (d) 5 spoke rounded; (e) 5 spoke closed; (f) 5 spoke outer covered; (g) 5 spoke inner covered; (h) 10 spoke; (i) 10 spoke fan.

3.2.5. Effects of rounding spoke edges

3.2.5.1. Front plane

Negligible differences exist between the 5 Spoke Sharp and 5 Spoke Rounded wheels in the vorticity, total pressure coefficient, local drag coefficient plots, and the average local drag coefficient. Therefore, rounding the spoke edges has no effect on the shoulder vortex's drag at this location.

3.2.5.2. Midway plane

Rounding the edges of the 5 Spoke wheel results in the local drag coefficient in the upper half of region 2 to reduce.

The 5 Spoke Sharp wheel exhibits a typical jetting vortex of positive vorticity whereas the 5 Spoke Rounded wheel exhibits this positive vorticity (the jetting vortex), but also a region of negative vorticity adjacent to this jetting vortex. As described above, this negative vorticity reduces the drag coefficient of the jetting vortex.

Overall, the average local drag coefficient of the 5 Spoke Rounded Wheel is 20 % lower than the 5 Spoke Sharp wheel.

3.2.5.3. Back plane

Little difference in the vorticity exists between the 5 Spoke Sharp and 5 Spoke Rounded wheels. However, the

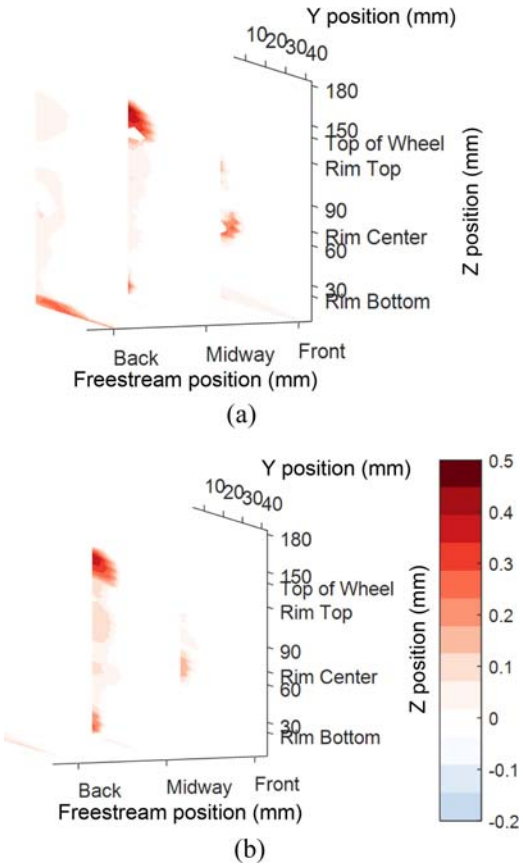

Figure 11. Approximate crossflow drag coefficient: (a) Covered treaded; (b) 5 spoke sharp.

direction of the flow is very different between the two wheels; the crossflow in the back plane of the 5 Spoke Sharp wheel has a far lower velocity in general than the crossflow in the back plane of the 5 Spoke Rounded wheels. The crossflow in the top half of the back plane of the 5 Spoke Rounded wheel moves quickly towards the vehicle indicating some flow reattachment.

The average local drag coefficient of these two wheels are almost the same, which agrees with the minor differences occurring in the vorticity, total pressure coefficient, and local drag coefficient in this plane.

3.2.6. Effects of tread pattern

3.2.6.1. Front plane

The Covered Slick wheel has greater vorticity than the Covered Treaded wheel. Furthermore, the total pressure coefficient deficit of the Covered Slick wheel extends over a greater area than the Covered Treaded wheel, however the magnitude of this deficit is typically less than the Covered Treaded wheels' deficit. The local drag coefficient plots in Figure 10 show that, these differences result in the Covered Slick wheel producing slightly more drag, which also agrees with the averaged local drag coefficients presented in Table 2.

3.2.6.2. Midway plane

In region 2 of the midway plane, Figures 8 (a) and (b), the Covered Slick wheel exhibits almost solely negative vorticity, while the Covered Treaded wheel has a combination of positive and negative vorticity. In addition, the vorticity formed in region 2 of the Covered Slick wheel is noticeably lower than the vorticity formed in region 2 of the Covered Treaded wheel. One further difference occurs in region 2 between these two wheels; the total pressure coefficient deficit and the local drag coefficient of the Covered Treaded wheel extend further down than the Covered Slick wheel, resulting in regions 2 and 3 joining.

A vortex occurs in region 3 of both wheels, which the authors identify as the jetting vortex, however, while the Covered Treaded wheel's jetting vortex is of the expected sign, positive, the Covered Slick wheel's jetting vortex is of the opposite sign to what is expected. Interestingly, the negative vorticity found in region 3 of the Covered Slick wheel results in more favourable total pressure and local drag coefficients than the Covered Treaded wheel.

The Covered Slick wheel's average local drag coefficient is almost the same as the Covered Treaded wheel's average local drag coefficient.

3.2.6.3. Back plane

At approximately the rim center in the back plane, the Covered Slick wheel exhibits a higher absolute vorticity than the Covered Treaded wheel. In addition, the direction of the flow is markedly different, with the fluid flowing away from the Covered Slick wheel much more than the

Table 2. Average local drag coefficient (dimensionless) of each rotating wheel's wake survey planes.

Wheel configuration	Front plane local drag coefficient average	Midway plane local drag coefficient average	Back plane local drag coefficient average
Covered slick	0.092	0.238	0.264
Covered treaded	0.075	0.244	0.248
5 spoke sharp	0.063	0.369	0.293
5 spoke rounded	0.072	0.295	0.298
5 spoke closed	0.087	0.290	0.282
5 spoke outer covered	N/A	0.274	0.270
5 spoke inner covered	0.076	0.306	0.270
10 spoke	0.081	0.342	0.305
10 spoke fan	0.079	0.350	0.336

Covered Treaded wheel. In addition, the Covered Slick wheel has slightly less flow separation than the Covered Treaded wheel, given the total pressure coefficient values. The Covered Slick wheel's lobe 2 in the local drag coefficient plot is noticeably larger and of a greater magnitude than the Covered Treaded wheel's lobe 2.

The beneficial effects of the negative vortex in the Covered Slick wheel's region 3 of the midway plane continue downstream; the total pressure coefficient and local drag coefficient of the Covered Slick wheel near the ground of the back plane are more favourable than the Covered Treaded wheel.

The Covered Slick wheel has a slightly higher average drag coefficient than the Covered Treaded wheel.

4. DISCUSSION

4.1. Validity of Reduced Reynolds Number Results

Berg and Brandt (2018) investigated the effects of certain rim geometric features on a full-scale vehicle at a Reynolds number of 12.8×10^6, and, where applicable, very similar trends were found between this study and that study. For example, the effects of coverage area were markedly similar, both in the effects on the flow field and the overall effect on the drag coefficient; the 5 Spoke Sharp wheel (33 % coverage area) had a 14 count greater drag coefficient than the Covered Treaded wheel (100 % coverage area). Berg and Brandt (2018) found that reducing the coverage area from 100 % to 40 % yielded a 17 count increase in the drag coefficient. Therefore, the trends found at the Reynolds number tested are valid for higher Reynolds numbers as well.

4.2. Effects of Wheel Rotation

4.2.1. Front plane

The reason why wheel rotation increases the roundedness of the flow features in the front plane is likely due to the change in the stagnation point's location at the front of the wheel (Mercker *et al*., 1991). As a result, it is expected that the flow around the shoulder occurs higher up on the rotating wheel.

4.2.2. Overall effect of wheel rotation

The effect of rotation on the average local drag coefficient of the Covered Slick wheel agrees with the force measurements results, as depending on the plane, it is either unaffected or significantly reduced. Therefore, this shows that at least part of the reduction in the drag coefficient with rotation arises from the front wheel.

The effect of rotation on the average local drag coefficient of the 5 Spoke Sharp wheel does not entirely agree with the force measurements results. While rotation reduces this parameter in the back plane, it greatly increases it in the midway plane. This suggests that, the reduction caused by rotation on the overall drag coefficient (as presented in the force measurements section) is either caused by the rear wheels or by non-local effects. These findings agree with literature, as the effects of front wheel rotation are varied (Wickern and Lindener, 2000; Elofsson and Bannister, 2002; Koitrand and Rehnberg, 2013). Furthermore, the different effects of rotation on these two wheels gives insight into why varied results pertaining to the effects of rotation on the drag coefficient have been reported.

4.3. Effects of Rim Opening

4.3.1. Front plane

Covering the rim typically increases the average local drag coefficient in this plane.

4.3.2. Midway plane

It is suggested that more flow separation occurs over the open rims than the covered rims because the flow can go through the open rims, whereas there is no flow going through the covered rims to alleviate any pressure differences caused by the separated flow thereby keeping the flow closer to the covered rim.

It is also suggested that openings in the rim near the rim track helps feed the jetting vortex and lower wake in general, thereby increasing the jetting vortex's drag. This would also explain Landström's (2011) findings pertaining to the location of coverage.

4.3.3. Back plane

The reason for the differences in vorticity, flow direction, and total pressure coefficient deficit found in the back plane is likely due to the difference in how the flow in the wheelhouse and around the wheel joins the flow around the vehicle; open rims allow some of the flow in the wheelhouse and around the inside of the wheel to escape through to the main flow through the rim openings, whereas, the flow behind a covered wheel can only join the main flow after the entire wheel has been passed.

4.3.4. Overall effects of rim opening on the drag coefficient

The conclusions that covering a rim greatly reduces the average local drag coefficient in the midway and back planes agree well with the trend found in the force measurements, whereby covering a rim typically reduces the overall drag coefficient of the vehicle.

4.4. Effects of 10 Spoke Fan Configuration

4.4.1. Overall effect of the fan spokes

The increase in the average local drag coefficient in the back plane is only 10 %, therefore, it is unlikely that the higher crossflow drag is the only cause of the poor drag coefficient presented in the force measurements section. Therefore, it is likely that the rear wheels and other regions of the vehicle contribute to the poor performance as well.

Furthermore, the other side of the vehicle may have a different flow field, as the rim is pulling air into the wheelhouse. Investigating the effects of different fan configurations on both the left and right sides of the vehicle is a recommendation for future research.

4.5. Effects of Rounding Spoke Edges

4.5.1. Midway plane

The reduction in the local drag coefficient in the upper half of region 2 corresponds to the point where the spokes have the greatest velocity relative to the freestream. Therefore, the lower local drag coefficient is a reasonable result as, while a sharp-edge cylinder (in this case the sharp spoke) has a Reynolds number-independent separation line, a rounded-edge cylinder (in this case the rounded spoke) has a Reynolds number-dependent separation line. As a result of this dependency, increasing the Reynolds number allows the flow to stay attached further around the cylinder, and thereby reducing the wake size and the drag (Tamura *et al*., 1998). In addition, rounding the edges of a square cylinder also promotes flow reattachment, which has been shown to reduce the drag of a cylinder (Carassale *et al*., 2013, 2014); Therefore, this mechanism may also be the cause of the drag reduction.

4.5.2. Overall effects of rounding spoke edges

Overall, rounding the spoke edges reduces the average local drag coefficient, which agrees with the force measurements.

4.6. Effects of Tread Pattern

4.6.1. Front plane

Hobeika *et al*. (2018a) found in their simulations that the edge pattern creates small vortices around the tyre shoulder. The authors suggest that the edge pattern is, in part, responsible for these differences in vorticity, total pressure coefficient, local drag coefficient, and average local drag coefficient, but that the longitudinal grooves also are responsible, as these larger grooves are expected to channel the flow over the wheel in a different fashion to the Covered Slick wheel. This would in turn affect the shoulder vortex.

4.6.2. Overall effects of tread pattern

The minor changes in the average local drag coefficient between the Covered Slick and Covered Treaded wheels agree with the minor difference in the vehicle's drag coefficient presented in the force measurements section.

5. CONCLUSION

The effects of rotation, rim coverage area, fan spokes, spoke sharpness, and tread pattern on the flow field and the drag coefficient of a vehicle were investigated. A 1/5th scale passenger vehicle was used for the investigation. The flow speed was chosen such that the effects measured on this scale model were indicative of a full-scale vehicle. Force measurements were taken with the nine investigated wheels stationary and rotating. Wake surveys were taken at three different planes for all wheel configurations while rotating, and for two wheel configurations while stationary. These planes were focussed around the front right wheel.

Wheel rotation reduced the vehicle's drag coefficient of all of the wheels investigated. Typically, rotation made the wheels produce more similar drag coefficients than when stationary. No trend between the coverage area and the effect of wheel rotation on the drag coefficient was found. However, the effects of wheel rotation on the flow field differed between the covered and open rims; rotating the front wheels reduced the jetting vortex's local drag coefficient of both covered and open wheels. However, rotating the open wheels increased the local drag coefficient from the wheel center to the upper rim track.

As also reported in literature (Landström, 2011), it was found in this study that, reducing the rim coverage area of a rotating wheel increased a vehicle's drag coefficient. This study also identified that this relationship held true for stationary wheels as well.

The fan-type spoke wheel greatly increased the vehicle's drag coefficient, compared to a square spoke wheel. Some changes in the vorticity and the total pressure coefficient between these two types of spoked rims were found. The only noteworthy change in the local drag coefficient arose from the increased crossflow velocity at the back of the front wheel.

Rounding the spoke edges of a rim resulted in almost no change in the drag coefficient of a vehicle with stationary wheels. However, a 5 count reduction was measured for rotating wheels. This reduction was due, in part, to a reduced jetting vortex drag coefficient. Furthermore, it was found that rounding the spoke edges reduced the local drag coefficient from the center of the wheel to the upper rim track.

The tread pattern had no effect on the vehicle when the wheels were stationary, however, it increased the drag coefficient by 2 counts when the wheels were rotating.

ACKNOWLEDGEMENT–This work is funded by FFI (Fordonsstrategisk Forskning och Innovation, Strategic Vehicle Research and Innovation) through Energymyndigheten (Swedish Energy Agency). The authors greatly appreciate their support. The authors would like to acknowledge Volvo Cars for providing the test vehicle, access to the wind tunnel facilities, and equipment.

REFERENCES

Aeroprobe Corporation (2015). Multi-hole Probes User Manual.

Arora, P. and Lyu, Z. (2016). *Aerodynamic Wind Tunnel in Passenger Car Application*. M. S. Thesis. Chalmers

University of Technology. Gothenburg, Sweden.

Barnard, R. H. (2001). *Road Vehicle Aerodynamic Design*. 2nd edn. Mechaero Publishing. St Albans, UK.

Berg, H. and Brandt, A. (2018). *Investigation of Aerodynamic Wheel Design*. M. S. Thesis. Chalmers University of Technology. Gothenburg, Sweden.

Brune, G. W. (1994). Quantitative low-speed wake surveys. *J. Aircraft* **31**, **2**, 249–255.

Carassale, L., Freda, A. and Marrè-Brunenghi, M. (2013). Effects of free-stram turbulence and corner shape on the galloping instability of square cylinders. *J. Wind Engineering and Industrial Aerodynamics* **123**, **Part B**, 274–280.

Carassale, L., Freda, A. and Marrè-Brunenghi, M. (2014). Experimental investigation on the aerodynamic behavior of square cylidners with rounded corners. *J. Fluids and Structures*, **44**, 195–204.

Cogotti, A. (2008). Evolution of performance of an automotive wind tunnel. *J. Wind Engineering and Industrial Aerodynamics* **96**, **6-7**, 667–700.

Council of European Union (2014). Regulation (EU) No 333/2014 of the European Parliament and of the Council. https://eur-lex.europa.eu/legal-content/EN/TXT/?uri=uriserv%3AOJ.L_.2014.103.01.0015.01.ENG

Croner, E., Bezard, H., Sicot, C. and Mothay, G. (2013). Aerodynamic characterization of the wake of an isolated rolling wheel. *Int. J. Heat and Fluid Flow*, **43**, 233–243.

D'Hooge, A., Palin, R. B., Johnson, S., Duncan, B. and Gargoloff, J. I. (2012). The aerodynamic development of the tesla model S - Part 2: Wheel design optimization. *SAE Paper No*. 2012-01-0178.

Elofsson, P. and Bannister, M. (2002). Drag reduction mechanisms due to moving ground and wheel rotation in passenger cars. *SAE Paper No*. 2002-01-0531.

Hassan, E. R., Lau, T. C. W. and Kelso, R. M. (2007). *Accuracy of Circulation Estimation Schemes Applied to Discretised Velocity Field Data*. *Proc. 16th Australasian Fluid Mechanics Conf.*, Gold Coast, Australia.

Hobeika, T. and Sebben, S. (2018a). CFD investigation on wheel rotation modelling. *J. Wind Engineering and Industrial Aerodynamics*, **174**, 241–251.

Hobeika, T. and Sebben, S. (2018b). Tyre pattern features and their effects on passenger vehicle drag. *SAE Paper No*. 2018-01-0710.

Hobeika, T., Sebben, S. and Landström, C. (2013). Investigation of the influence of tyre geometry on the aerodynamics of passenger cars. *SAE Paper No*. 2013-01-0955.

Hucho, W. H. (1998). *Aerodynamics of Road Vehicles*. 4th edn. SAE International. Warrendale, Pennsylvania, USA.

Huminic, A. and Huminic, G. (2017). Aerodynamic study of a generic car model with wheels and underbody diffuser. *Int. J. Automotive Technology* **18**, **3**, 397–404.

Koitrand, S. and Rehnberg, S. (2013). *A Computational Investigation of Wheel and Underbody Flow Interaction*. M. S. Thesis. Chalmers University of Technology. Gothenburg, Sweden.

Landström, C. (2011). *Passenger Car Wheel Aerodynamics*. Ph. D. Dissertation. Chalmers University of Technology. Gothenburg, Sweden.

Maskell, E. C. (1973). Progress Towards a Method for the Measurement of the Components of the Drag of Wing of Finite Span. Royal Aircraft Establishment Technical Report 72232.

Mercker, E., Breuer, N., Berneburg, H. and Emmelmann, H. J. (1991). On the aerodynamic interference due to rolling wheels of passenger cars. *SAE Paper No*. 910311.

Qiu, Z. (2009). *Wheel Aerodynamic Developments by Module-based Prototype Rims and Stationary Rim Shields*. M. S. Thesis. Chalmers University of Technology. Gothenburg, Sweden.

Schewe, G. (2013). Reynolds-number-effects in flow around a rectangular cylinder with aspect ratio 1:5. *J. Fluids and Structures*, **39**, 15–26.

Schnepf, B. (2016). *Untersuchung von Einflussfaktoren auf die Umströmung eines Pkw-Rades in Simulation und Experiment*. Ph. D. Dissertation. Technischen Universität München. Munich. Germany.

Schnepf, B., Schütz, T. and Indinger, T. (2015). Further investigations on the flow around a rotating, isolated wheel and detailed tread pattern. *SAE Paper No*. 2015-01-1554.

Söderblom, D. (2012). *Wheel Housing Aerodynamics of Heavy Trucks*. Ph. D. Dissertation. Chalmers University of Technology. Gothenburg, Sweden.

Sternéus, J., Walker, T. and Bender, T. (2007). Upgrade of the Volvo cars aerodynamic wind tunnel. *SAE Paper No*. 2007-01-1043.

Tamura, T., Miyagi, T. and Kitagishi, T. (1998). Numerical prediction of unsteady pressure on a square cylinder with various corner shapes. *J. Wind Engineering and Industrial Aerodynamics*, **74-76**, 531–542.

Thivolle-Cazat, E. and Gilléron, P. (2006). Flow analysis around a rotating wheel. *Proc. 13th Int. Symp. Applications of Laser Techniques to Fluid Mechanics*, Lisbon, Portugal.

Wäschle, A., Cyr, S., Kuthada, T. and Wiedemann, J. (2004). Flow around an isolated wheel – Experimental and numerical comparison of two CFD codes. *SAE Paper No*. 2004-01-0445.

Wickern, G. and Lindener, N. (2000). The audi wind tunnel: Final design and first operational experience. *SAE Paper No*. 2000-01-0868.

Wu, J. C. (1982). A generalized wake-integral approach for drag determination in three-dimensional flows. *Proc. 17th Aerospace Sciences Meeting*, New Orleans, Louisiana, USA.